AIAA-2000-2062

LINEAR MODEL OF MACH WAVE SUPPRESSION IN A DUAL-STREAM JET

Dimitri Papamoschou*
Department of Mechanical and Aerospace Engineering
University of California, Irvine
Irvine, CA 92697-3975

Reduction of Mach wave emission from a dual-stream jet is modeled via a linear temporal analysis in the frame of reference of the jet instability. The interface between the primary and secondary streams is simulated by a flexible wavy wall with zero phase speed and arbitrary growth rate. The interface between the secondary and ambient streams is simulated by a vortex sheet. The secondary stream, which is adjacent to the wall, has variable Mach number and height. The semi-infinite ambient stream is supersonic. The study focuses on the case of a subsonic secondary stream and compares it to the case of uniform supersonic flow over the wall. It is found that a subsonic layer over the wall creates two effects: (a) the magnitude of the pressure disturbance on the wall is diminished and (b) the disturbance decays exponentially within the height of the layer. The pressure fluctuation that is finally transmitted into the supersonic stream is very weak, leading to considerable noise suppression. The noise reduction increases with decreasing value of the secondary Mach number and with increasing height of the secondary flow. These trends compare favorably with experimental results in which near-field noise was measured in dual-stream jets with variable secondary-flow Mach number and adjustable height of the secondary stream.

Introduction

For four decades now, efficient suppression of high-speed jet noise has been a challenging problem that has stymied development of supersonic commercial aircraft [1]. Supersonic jet noise consists of three main components: turbulent mixing noise, comprising the contribution of large-scale and fine-scale structures; broadband shock noise; and screech tones [2]. The latter two are present in imperfectly-expanded jets and can be theoretically eliminated by pressure matching the jet. Mixing noise is by far the most difficult to control. For exhaust speeds greater than about 500 m/s, large-scale mixing noise manifests itself primarily as Mach wave radiation, caused by the supersonic convection of turbulent eddies with respect to the ambient. In the vicinity of the potential core, Mach waves are very strong, non-linear pressure waves which decay into weak acoustic waves far from the jet. In high-speed, hot jets, Mach wave emission is the dominant source of sound and radiates in the aft quadrant.

The simplest way to explain Mach wave radiation is to consider the turbulent interface between the jet and the ambient as a wavy wall propagating at a constant convective speed U_c. When U_c is supersonic, Mach waves are radiated from the wall. The notion of sound radiation from large-scale flow instabilities was first confirmed in the supersonic jet experiments of McLaughlin et al. [3] and the subsequent experiments of Troutt & McLaughlin [4]. In those experiments, the orientation, wavelength, and frequency of the measured acoustic radiation were found to be consistent with the Mach wave concept outlined above. The linear stability analysis of Tam & Burton [5] further solidified this idea by showing that the sound emitted by a supersonic instability wave matched very well the aforementioned experimental data. Since then, a large volume of experimental and theoretical works have addressed multi-

*Professor, senior member AIAA

ple aspects of this problem. See for example Refs.[6], [7], [8], and [9].

The vast majority of silencing efforts for supersonic jets have focused on mixing enhancement, often combined with ejectors. Examples are the works by Westley & Lilley [10] and Seiner & Gilinki [11] on lobed nozzles; Ahuja & Brown [12], Zaman et al. [13], and Seiner & Grosh [14], on tabs; Samimy et al [15] on nozzle cutouts; and Strykowski et al. [16] on a counterflow method. The underlying principle is to enhance the axial decay of the velocity in the jet plume, hence reducing the length of the Mach-wave emitting region; at the same time, all the other sources of noise which depend on jet velocity (fine-scale, quadrupole) would also be reduced. Although such methods can produce significant increase in the jet spreading rate, reduction of mixing noise has been modest at best and occasionally the jet becomes louder. Moreover, the thrust loss induced by mechanical mixers in supersonic jets can easily reach the order of 10% [14, 18] which is unacceptable for the economic operation of an aircraft. Currently, the leading method for reducing supersonic jet noise is the mixer-ejector [17] which decelerates the jet exhaust by mixing it with entrained air inside a shroud. It provides very good noise reduction but the required shroud is very large, which adds significant drag and weight penalties on top of the mixer losses.

Recently, it has been demonstrated that adding a secondary flow around a supersonic jet can significantly reduce Mach wave emission [19, 20]. The conditions (speed and temperature) of the secondary flow are such as to render the motion of the jet eddies subsonic relative to the secondary flow, while maintaining the secondary-flow eddies subsonic relative to the ambient flow. The jet instability wave becomes intrinsically subsonic, even though the absolute speed of the instability, as seen by a fixed observer, remains supersonic. The method is called "Mach Wave Elimination" in the sense that the strong shock/expansion waves formed around the jet eddies (which farther out become Mach waves) no longer exist. In a strict sense, however, Mach wave emission still occurs because an observer fixed in the ambient fluid still feels supersonically-traveling sources of sound (i.e., Mach waves), but at a much reduced level. The conditions of the secondary flow for Mach Wave Elimination are based on empirical models for the convective velocity U_c, derived from direct measurements of U_c in jets and shear layers [21, 22]. So far, the way this technique has been

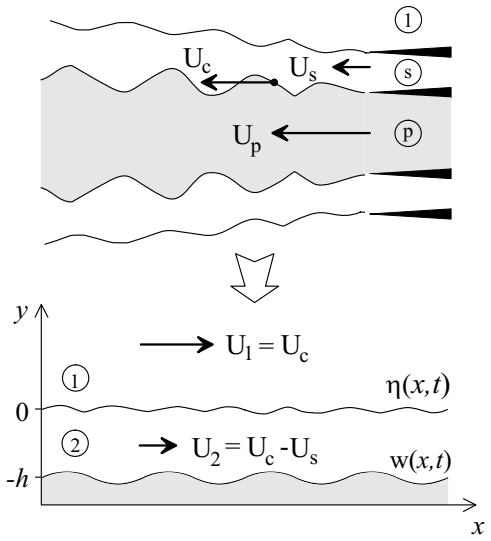

Fig.1 Transformation from laboratory coordinate system to coordinate system moving with the jet instability.

presented in various publications suggests a "on-off" approach to noise reduction: if the instability is intrinsically subsonic we get a certain level of noise reduction and if it is supersonic we do not. One expects, however, a more gradual dependence of noise reduction on Mach number. Furthermore, the effect of the thickness of the secondary flow has not been addressed.

The purpose of this paper, therefore, is to explain at the most fundamental level the sound reduction obtained when a secondary flow is added around a supersonic jet. Quantitative prediction of Mach wave emission is beyond the scope and means of this work; this has been done by other investigators in the past, using very sophisticated analytical and numerical techniques. Noted in this vein are the works by Morris & Dahl ([23, 24]) in which the instability wave model was used to predict noise emission from coaxial supersonic jets. However, those papers focused on supersonic instabilities and did not cover the condition where an instability becomes intrinsically subsonic by proper conditioning of the secondary flow. The emphasis of the present paper is derivation of a simple physical model that would capture the physics of *noise reduction* associated with the addition of a secondary flow.

Analysis

Model Description

The purpose of the model is to capture the essen-

tial physics of Mach wave suppression from a dual-stream jet while ignoring the other noise sources. Figure 1(a) presents a cartoon of this jet, seen in the laboratory frame of reference. The primary and secondary velocities are U_p and U_s, respectively. Absent a secondary stream, Mach wave radiation is governed by the convective velocity U_c of the jet eddies, which are treated here as an instability wave. When U_c is supersonic with respect to the ambient fluid, the disturbances generated by the instability propagate along Mach waves very far into the ambient fluid, causing a substantial source of noise. Addition of a secondary stream changes the Mach number felt by the jet eddies and creates a new interface, between the secondary and ambient flows, which needs to be modeled.

To reduce the problem to its simplest elements, we perform the transformation shown in Fig. 1(b). We model the jet instability as a wavy, flexible wall and "ride" with it. Without sacrificing the basic physics of the problem, we assume a planar flow because its solution is much simpler than that of the axisymmetric flow, thereby giving better insight into the fundamental mechanisms. In this Lagrangian frame of reference, which travels with velocity U_c, the wall instability is stationary and grows in time. Adjacent to the wall is the secondary stream (now denoted "2" instead of "s") with velocity $U_2 = U_c - U_s$ and of height h. Further away is the ambient stream (1) with velocity $U_1 = U_c$. The ambient and secondary streams are separated by a vortex sheet which evolves in time. This arrangement obviates the need to solve for the primary jet instability; instead, we assume a phase velocity U_c and a growth rate. The phase speed will take values which are realistic for actual jets, as determined by experiments. The growth rate will be assigned a variety of values to determine its effect on noise reduction. We will see later that noise reduction is not very sensitive on the growth rate.

Problem definition

We consider the temporal problem of an inviscid vortex sheet between streams 1 and 2, the lower stream (2) being bounded by a flexible wall of shape

$$w(x,t) \;=\; \delta e^{i\beta(x-st)} \tag{1}$$

where δ is the amplitude (real), β is the wavenumber (real) and s is the phase speed (complex). For the case of a growing disturbance with zero phase speed, $s = 0 + is_i$, where s_i is the temporal growth rate. The vortex sheet between the secondary and ambient streams is modeled by the addition of two waveforms

$$\eta(x,t) \;=\; \epsilon e^{i\alpha(x-ct)} \;+ \nu e^{i\beta(x-st)} \tag{2}$$

The first waveform describes the motion of the vortex sheet that would have occurred if there were no wall present or if the wall were flat, i.e., in the absence of a wavenumber imposed by boundary conditions. This is the well-known problem of the Kelvin-Helmholtz instability, first solved for compressible flow by Landau [25] for an unbounded vortex sheet. The amplitude ϵ (real) and wavenumber α (real) of this motion are arbitrary, whereas the complex phase speed c is determined from the eigensolution. The second waveform represents the reaction of the interface to the wavy wall. Its wavenumber and growth rate are identical to those of the wall, but its complex amplitude ν is unknown and will be determined by the boundary conditions. The imaginary part of ν accounts for the phase shift of a disturbance as it travels from the wall to the vortex sheet.

General solution

The perturbation velocity potential $\phi_j(x,y,t)$ is governed by

$$\frac{D^2\phi_j}{Dt^2} \;=\; a_j^2 \nabla^2 \phi_j \tag{3}$$

where

$$\frac{D}{Dt} \;\equiv\; \frac{\partial}{\partial t} + U_j \frac{\partial}{\partial x}$$

Subscript j takes the values of 1 and 2, corresponding to the outer and inner streams, respectively. We assume a solution of the form

$$\phi_j(x,y,t) \;=\; \psi_j(y) e^{i\alpha(x-ct)} \;+\; \zeta_j(y) e^{i\beta(x-st)} \tag{4}$$

which is amenable to the boundary conditions on the wall and at the interface. Substituting in Eq. 3, we obtain ordinary differential equations for the four eigenfunctions of this problem:

$$\begin{aligned} \frac{d^2\psi_j}{dy^2} \;&=\; \alpha^2 \sigma_j^2 \psi_j \\ \\ \frac{d^2\zeta_j}{dy^2} \;&=\; \beta^2 \xi_j^2 \zeta_j \end{aligned} \tag{5}$$

where

$$\begin{aligned} \sigma_j^2 \;&\equiv 1 - \left(\frac{U_j - c}{a_j}\right)^2 \\ \\ \xi_j^2 \;&\equiv 1 - \left(\frac{U_j - s}{a_j}\right)^2 \end{aligned} \tag{6}$$

The general solutions to Eq. 5 are

$$\begin{aligned} \psi_j(y) &= A_j e^{\alpha\sigma_j y} + B_j e^{-\alpha\sigma_j y} \\ \zeta_j(y) &= D_j e^{\beta\xi_j y} + E_j e^{-\beta\xi_j y} \end{aligned} \tag{7}$$

where the coefficients A_j, B_j, D_j, and E_j are to be determined from the boundary conditions. Hence, the general solution for the velocity potential is

$$\begin{aligned} \phi_j(x,y,t) = \quad & \left(A_j e^{\alpha\sigma_j y} + B_j e^{-\alpha\sigma_j y}\right) e^{i\alpha(x-ct)} \\ & + \left(D_j e^{\beta\xi_j y} + E_j e^{-\beta\xi_j y}\right) e^{i\beta(x-st)} \end{aligned} \tag{8}$$

Boundary and boundedness conditions

The requirement of boundedness at $y = \infty$ requires zeroing of the coefficients multiplying the terms that grow exponentially with y in Eq. 8, i.e., $A_1 = 0$ and $D_1 = 0$. If σ_1 and ξ_1 were purely imaginary (the case of a supersonic neutral disturbance), A_1 and D_1 must still be zero because they multiply terms describing left-running waves which are not physically present in this problem.

The wall boundary condition at $y = -h$ dictates

$$\left(\frac{\partial\phi_2}{\partial y}\right)_{y=-h} = \frac{Dw}{Dt}$$

Substituting the general solution for ϕ_2 from Eq. 8 and the wall shape from Eq. 1, we obtain

$$\begin{aligned} & \alpha\sigma_2 \left[A_2 e^{-\alpha\sigma_2 h} - B_2 e^{\alpha\sigma_2 h}\right] e^{i\alpha(x-ct)} \\ & + \beta\xi_2 \left[D_2 e^{-\beta\xi_2 h} - E_2 e^{\beta\xi_2 h}\right] e^{i\beta(x-st)} \\ & = i\delta\beta(U_2 - s) e^{i\beta(x-st)} \end{aligned}$$

which gives

$$A_2 e^{-\alpha\sigma_2 h} - B_2 e^{\alpha\sigma_2 h} = 0 \tag{9}$$

$$D_2 e^{-\beta\xi_2 h} - E_2 e^{\beta\xi_2 h} = i\delta\frac{U_2 - s}{\xi_2} \tag{10}$$

Continuity of the flow at the interface $y = 0$ requires

$$\left(\frac{\partial\phi_j}{\partial y}\right)_{y=0} = \frac{D\eta}{Dt}$$

Substituting the general solution for ϕ_j from Eq. 8 and the interface shape from Eq. 2, we have

$$\begin{aligned} & \alpha\sigma_j(A_j - B_j) e^{i\alpha(x-ct)} + \beta\xi_j(D_j - E_j) e^{i\beta(x-st)} = \\ & \qquad \epsilon i\alpha(U_j - c) e^{i\alpha(x-ct)} + i\nu\beta(U_j - s) e^{i\beta(x-st)} \end{aligned}$$

which spawns the four relations

$$-\sigma_1 B_1 = i\epsilon(U_1 - c) \tag{11}$$

$$\sigma_2(A_2 - B_2) = i\epsilon(U_2 - c) \tag{12}$$

$$-\xi_1(E_1) = i\nu(U_1 - s) \tag{13}$$

$$\xi_2(D_2 - E_2) = i\nu(U_2 - s) \tag{14}$$

At the interface $y = 0$ we also require pressure balance, $p_1' = p_2'$. The pressure fluctuation is given by $p' = -\rho D\phi/Dt$, thus

$$\rho_1\frac{D\phi_1}{Dt} = \rho_2\frac{D\phi_2}{Dt}$$

Inserting the general solution for ϕ_1 and ϕ_2 given by Eq. 8,

$$\begin{aligned} & \rho_1[B_1 i\alpha(U_1 - c)e^{i\alpha(x-ct)} \\ & \quad + E_1 i\beta(U_1 - s)e^{i\beta(x-st)}] \\ & = \rho_2[(A_2 + B_2)i\alpha(U_2 - c)e^{i\alpha(x-ct)} \\ & \quad + E_2 i\beta(U_2 - s)e^{i\beta(x-st)}] \end{aligned}$$

Matching the coefficients of each exponential term, we obtain

$$\frac{B_1}{A_2 + B_2} = \frac{\rho_2}{\rho_1}\frac{U_2 - c}{U_1 - c} \tag{15}$$

$$\frac{E_1}{D_2 + E_2} = \frac{\rho_2}{\rho_1}\frac{U_2 - s}{U_1 - s} \tag{16}$$

Eigenvalue problem

Combining Eqs. 11, 12, and 15, we arrive at the eigenvalue problem for the Kelvin-Helmholtz component of the vortex-sheet motion (first term on the right hand side of Eq. 2.)

$$\frac{\rho_2}{\rho_1}\frac{\sigma_1}{\sigma_2}\left(\frac{U_2 - c}{U_1 - c}\right)^2 \frac{1 + B_2/A_2}{1 - B_2/A_2} = -1$$

This is the problem of a vortex sheet developing in the absence of a geometrically-imposed wavenumber. We now define

$$\mu_j \equiv \frac{U_j - c}{a_j} \tag{17}$$

as the complex convective Mach number of the vortex sheet. Using the relation $a^2 = \gamma p/\rho$, the eigenvalue relation is cast in the form

$$\left(\frac{\gamma_2}{\gamma_1}\right)^2 \mu_2^4(1 - \mu_1^2) - \left[\frac{1 - B_2/A_2}{1 + B_2/A_2}\right]^2 \mu_1^4(1 - \mu_2^2) = 0$$

where the term inside the square brackets describes the influence of a flat wall on the instability of the vortex sheet and equals, from Eq. 9, $\tanh(\alpha h\sqrt{1 - \mu_2^2})$. For an unbounded vortex sheet

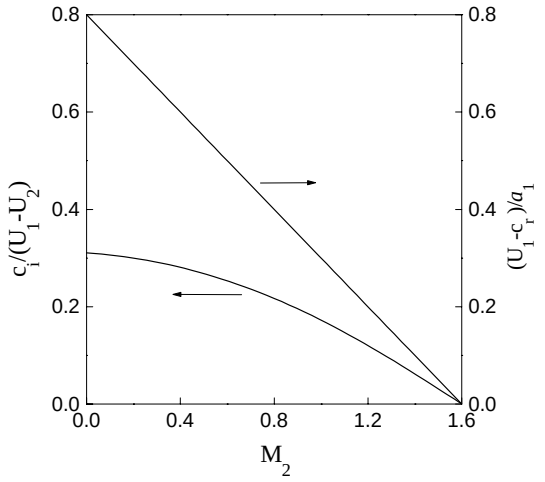

Fig.2 Convective Mach number and amplification rate of vortex sheet between $M_1 = 1.6$ and variable M_2.

$(h = \infty)$, this terms equals 1.0. The eigenvalue problem becomes

$$\left(\frac{\gamma_2}{\gamma_1}\right)^2 \mu_2^4(1-\mu_1^2) - \tanh^2\left[\alpha h\sqrt{1-\mu_2^2}\right]\mu_1^4(1-\mu_2^2) = 0 \tag{18}$$

From the definition of Eq. 17, the relation between μ_1 and μ_2 is

$$\mu_2 = \frac{a_1}{a_2}\left[\mu_1 - M_1\left(1 - \frac{U_2}{U_1}\right)\right] \tag{19}$$

Equations 18 and 19 were solved simultaneously using a complex Newton-Raphson method to find the roots of Eq. 18. The complex phase speed $c = c_r + ic_i$ and the variables σ_j were thus determined. Figure 2 plots the normalized growth rate $c_i/(U_2 - U_1)$ and the convective Mach number $(U_1 - c_r)/a_1$ versus M_2 for $M_1 = 1.6$ and uniform density. The convective Mach number is subsonic throughout, hence this motion of the vortex sheet does not radiate Mach waves. The phase speed is very close to the average of the freestream velocities.

Determination of the coefficients

We are now able to solve for all the coefficients of Eq. 8. Those for the outer flow are already known. For the inner flow, A_2 and B_2 are obtained by solving simultaneously Eqs. 9 and 12; D_2 and E_2 are obtained by solving simultaneously Eqs. 10 and 14. The expressions for all the coefficients are shown in Table 1. Finally, substituting E_1 and E_2 into Eq. 16, we obtain the amplitude of the second component of the vortex-sheet motion

$$\nu = \delta\left[\cosh\beta\xi_2 h + \frac{\rho_1\xi_2}{\rho_2\xi_1}\left(\frac{U_1 - s}{U_2 - s}\right)^2 \sinh\beta\xi_2 h\right]^{-1} \tag{20}$$

This is an important relation as it describes the attenuation effect of the inner stream on a disturbance generated on the wall. Some special cases are worth noting. For zero flow velocity ($M_1 = M_2 = 0$) and uniform density, Eq. 20 gives $\nu = \delta e^{-\beta h\sqrt{1+(s_i/a)^2}}$, i.e, an exponential decay governed by the "growth Mach number" s_i/a; the larger the growth rate, the faster the decay. When the height of the inner stream is reduced to zero ($h = 0$), we obtain $\nu = \delta$, as expected. For $M_1 = M_2 > 1$, zero wall growth, and uniform density, $\nu = \delta e^{-i\lambda\beta h}$ where $\lambda = \sqrt{M_2^2 - 1}$, that is, the interface has the same amplitude as the wall but with a phase change that accounts for the signal propagation along characteristics.

Table 1 Coefficients of Eq. 8

Outer Solution	Inner Solution
$A_1 = 0$	$A_2 = i\dfrac{U_2 - c}{\sigma_2}\dfrac{\epsilon}{1 + e^{-2\alpha\sigma_2 h}}$
$B_1 = -i\epsilon\dfrac{U_1 - c}{\sigma_1}$	$B_2 = i\dfrac{U_2 - c}{\sigma_2}\dfrac{\epsilon}{1 + e^{2\alpha\sigma_2 h}}$
$D_1 = 0$	$D_2 = i\dfrac{U_2 - s}{\xi_2}\dfrac{\nu e^{\beta\xi_2 h} - \delta}{e^{\beta\xi_2 h} - e^{-\beta\xi_2 h}}$
$E_1 = -i\nu\dfrac{U_1 - s}{\xi_1}$	$E_2 = i\dfrac{U_2 - s}{\xi_2}\dfrac{\nu e^{-\beta\xi_2 h} - \delta}{e^{\beta\xi_2 h} - e^{-\beta\xi_2 h}}$

Calculation of the pressure field

The pressure fluctuation is $p' = -\rho D\phi/Dt$, which here becomes

$$\begin{aligned} p_j'(x,y,t) &= -i\rho_j\left[\alpha(U_j - c)\psi_j(y)e^{i\alpha(x-ct)}\right. \\ &+ \left.\beta(U_j - s)\zeta_j(y)e^{i\beta(x-st)}\right] \end{aligned} \tag{21}$$

with $j = 2$ for $-h < y < 0$ and $j = 1$ for $y > 0$. Only the real part of Eq. 21 gives the actual pressure field. The plots that follow depict the pressure fluctuation for fixed $M_1 = 1.6$ and variable M_2 and h. The density field is uniform and $\gamma_1 = \gamma_2 = 1.4$. Note that setting $M_2 = M_1$ is equivalent to setting $h = 0$, i.e., the case of no secondary flow. Other parameters are $\beta = 1$, $\delta = 0.01$, $s_i/a_1 = 0.05$, $\alpha = 1$, $\epsilon = 0.01$, and non-dimensional time $t\beta U_1 = 1.0$. It was ensured that the maximum slopes of the wall

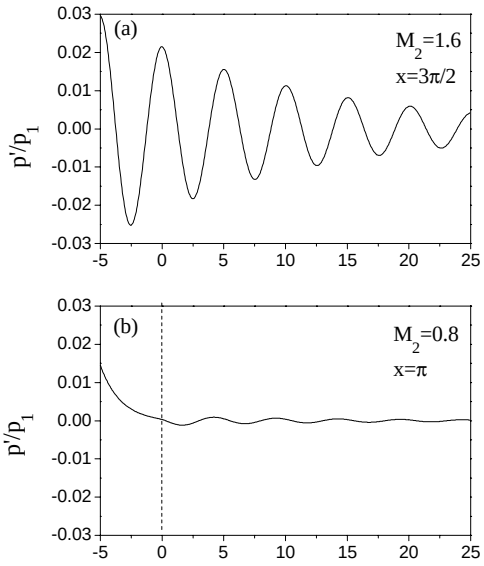

Fig.3 Fluctuating pressure versus transverse distance for M_1=1.6 and for (a) M_2=1.6 (no secondary flow); and (b) M_2=0.8. Dashed line indicates location of vortex sheet.

and vortex sheet were always less than 0.02 in order to be well within the limits of the linear assumption. Figure 3(a) shows the pressure fluctuation as a function of y for $M_2 = 1.6$ (the case of no secondary flow). The disturbance originates at $x = 3\pi/2$, a point of maximum slope therefore maximum compression for supersonic flow. The Mach wave radiation is evident. The slow decay of the radiation envelope is caused by the amplification rate of the wall, which introduces an exponential decay term in the solution for ϕ (Eq. 8). In Fig. 3(b) a subsonic layer with M_2=0.8 and thickness $\beta h = 5.0$ is introduced between the wall and the supersonic stream. To compare directly with the previous case, the disturbance origin has been shifted to $x = \pi$, a point of maximum compression for subsonic flow. Two important effects are noted. First, the magnitude of the disturbance on the wall diminishes substantially. This is particularly true when the height of the secondary stream is significantly larger than the wavelength of the wall. As $\beta h \to 0$, however, the wall pressure distribution approaches that of the supersonic case despite the presence of the subsonic layer. Second, the disturbance decays very rapidly with distance from the wall. The signal that finally emerges in the supersonic stream is very weak because of the combination of those two effects.

Sound reduction

In the typical acoustics experiment, a microphone is fixed at location (x, y) with respect to the jet nozzle and records the pressure fluctuation $p'(x, y, t)$. The sound pressure level is then derived from the root mean square (rms) value of signal. It is instructive to extract an analogous "sound measurement" from this analysis. In the problem of Fig. 1(b), where we are moving with the jet boundary, the microphone is located at fixed y and sweeps the flow from left to right, thus crosses the waves emitted by the wall. As the microphone moves, the amplitudes of the wall and vortex sheet motions grow exponentially and so does the magnitude of the pressure field. This artifact of the temporal problem prevents us from obtaining a legitimate rms value of the pressure recorded by our microphone. The problem can be circumvented by freezing time and calculating the rms value of the pressure as the microphone traverses a very large axial distance,

$$p_{\rm rms}(y,t) = \left[\lim_{L\to\infty}\frac{1}{2L}\int_{-L}^{L} p'^2(x,y,t)dx\right]^{1/2}$$

where $p'(x, y, t) = Re\{p_1(x, y, t)\}$, with $p_1(x, y, t)$ given by Eq. 21. This expression was evaluated computationally with $L = 200$ and $\alpha = \beta = 1$.

The sound pressure level (SPL, in decibels) is given by $20\log_{10}(p_{\rm rms}/p_{\rm ref})$, with $p_{\rm ref}$ a commonly accepted reference pressure. Supposing that we compare flow cases A and B at fixed time t_0, with B being the quieter flow, the SPL reduction is

$$\Delta{\rm SPL}(y) \;=\; 20\log_{10}\left(\frac{p_{{\rm rms}_A}(y,t_0)}{p_{{\rm rms}_B}(y,t_0)}\right)$$

Figure 4 plots ΔSPL versus non-dimensional distance βy for the cases depicted in Figs. 3(a) and 3(b) and for various wall growth rates. For $\beta y > 5$, the SPL reduction reaches a constant value. This is typical of many other cases examined. We consider therefore $\beta y > 5$ the "far field" in the context of sound reduction. Figure 4 shows that the far-field sound reduction is rather insensitive on wall growth rate. Variations of the other parameters of the problem (besides M_2 and βh), namely initial amplitudes of wall and vortex sheet, vortex sheet wavenumber, and time t, shows that the sound reduction is insensitive on those parameters too. Figure 5 depicts the effects of M_2 and βh on far-field sound reduction for $M_1 = 1.6$. Decreasing M_2 to subsonic values, and increasing βh, both have a substantial effect on sound reduction. The reader is cautioned that the noise reductions shown here consider only one element of supersonic jet noise – Mach wave radiation – and ignore other important noise components, namely

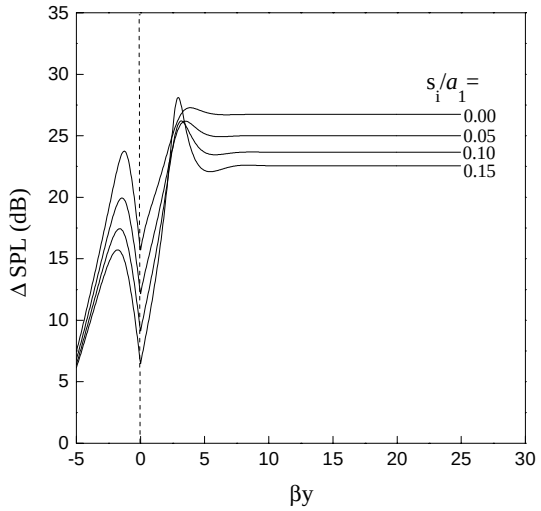

Fig.4 Sound reduction versus transverse distance for various wall amplification rates.

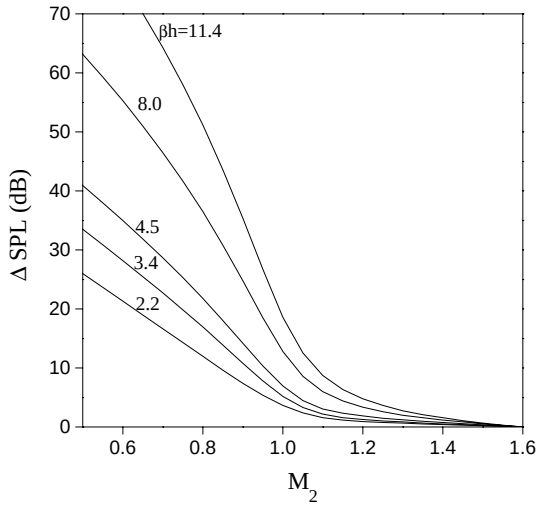

Fig.5 Theoretical dependence of sound reduction on M_2 and βh.

fine-scale noise and quadrupole emission. Although Mach wave radiation is the dominant source of noise in high-speed jets, the other noise components constitute a noise "floor" that is impenetrable even if Mach wave radiation were completely eliminated. Even if this floor were only 5% of the total noise (in terms of rms pressure fluctuation), the maximum possible reduction would be 26 dB.

Experiment

Apparatus

Experiments were conducted in a dual-stream, rectangular jet apparatus drawn in Fig. 6. The primary

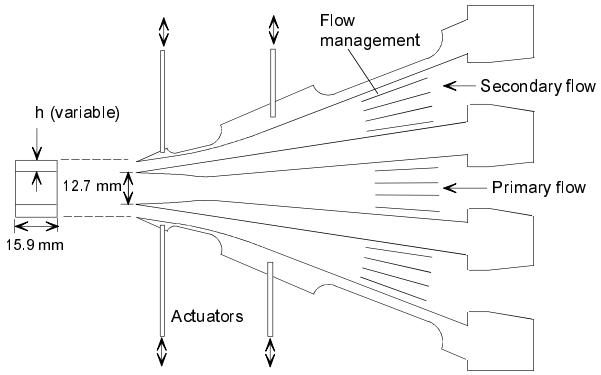

Fig.6 Rectangular supersonic jet with secondary flow of variable exit height and adjustable nozzle shape. Upstream actuators control the exit height; downstream actuators control the nozzle shape.

stream was supplied by an inner nozzle, designed by the method of characteristics for Mach number 1.5. Its exit dimensions were 12.7 mm in height and 15.9 mm in width. The secondary stream was supplied by two outer nozzles featuring flexible walls for adjustment of their exit height and contour. The width of the secondary stream was 15.9 mm (same as that of the primary stream). In the present experiments, only the upper secondary duct was used and its nozzle was set to be convergent. Mixtures of helium and air were supplied to both the primary and secondary streams, which exhausted into ambient, still air with speed of sound $a_1 = 345$ m/s. The mass fraction of helium in the primary stream was 26%, resulting in a mixture gas constant of 760 J/(kg°K). Supplied at a fully-expanded Mach number of 1.5, this mixture has a velocity of 700 m/s which is typical of the exhaust velocity of high-specific-thrust engines. The height of the secondary stream assumed the values of 2,3,4,7, and 10 mm. The Mach number of the secondary flow took the values M_s =0, 0.21, 0.40, 0.60, 0.75, 0.83, 0.90, and 1.00. For each M_s, the helium mass fraction of the secondary flow was adjusted so that the its exit density matched the density of the ambient air, hence simulating the flow of a fan stream in a turbofan engine.

The convective velocity of the jet eddies U_c was calculated from the empirical model proposed by Murakami & Papamoschou [22]. This model is based on direct measurements of U_c in shear layers and coaxial jets; its predictions match closely the convective velocity calculated from the slope of the Mach waves and inferred from the directivity of the acoustic field. For the jet without secondary flow, the convective velocity of the eddies was predicted to be 550 m/s, hence the Mach number in

the frame of reference of the instability (Fig. 1(b)) was $M_1 = U_c/a_1$=550/345=1.6. As the velocity of the secondary flow increases, the convective velocity of the jet eddies is calculated to undergo small variations which are not substantial for the theoretical aspects of this paper. Table 2 summarizes the Mach numbers and velocities of the experiment. The Reynolds number of the primary jet, based on its hydraulic diameter, was 400,000.

Table 2 Jet conditions

Case	M_p	U_p (m/s)	M_s	U_s (m/s)	M_1	M_2
A	1.5	700	0	0	1.6	1.6
B	1.5	700	0.21	75	1.6	1.4
C	1.5	700	0.40	140	1.6	1.2
D	1.5	700	0.60	210	1.6	1.0
E	1.5	700	0.75	260	1.6	0.8
F	1.5	700	0.83	290	1.6	0.7
G	1.5	700	0.90	315	1.6	0.6
H	1.5	700	1.00	345	1.6	0.5

Schlieren photography

A spark schlieren system with 20-nanosecond exposure (short enough to freeze the smallest details of the flow) was used to obtain qualitative images of the jets. The four photographs of Fig. 7 highlight the Mach wave emission and its reduction using certain combinations of secondary-flow Mach number and height. The microphone location for the sound measurements, discussed below, is visible. Figure 7(a) depicts the single jet (case A). A series of very strong, nearly organized Mach waves is evident, with finer Mach waves between the strong ones. Figure 7(b) depicts case G ($M_2 = 0.6$) with a secondary-stream height of 7 mm. With the relative Mach number subsonic and the secondary flow relatively thick, the Mach waves practically disappear from the image. A rough analogy would be the theoretical plot of Fig. 3(b), where the subsonic layer has produced a dramatic reduction of the signal emerging into the ambient fluid. In Fig. 7(c), the secondary-stream height stays the same (h = 7 mm) but the relative Mach number increases to 1.2 (case C). The Mach waves are distinct but weaker than in case A. Figure 7(d) depicts case G again but with a reduced secondary stream height of 3 mm. Mach waves, especially those close to the jet exit, are weaker and less sharp than those of Case A. The subsonic layer allows the disturbance to decay and spread, but the layer height is too small in this case to allow substantial attenuation of the signal.

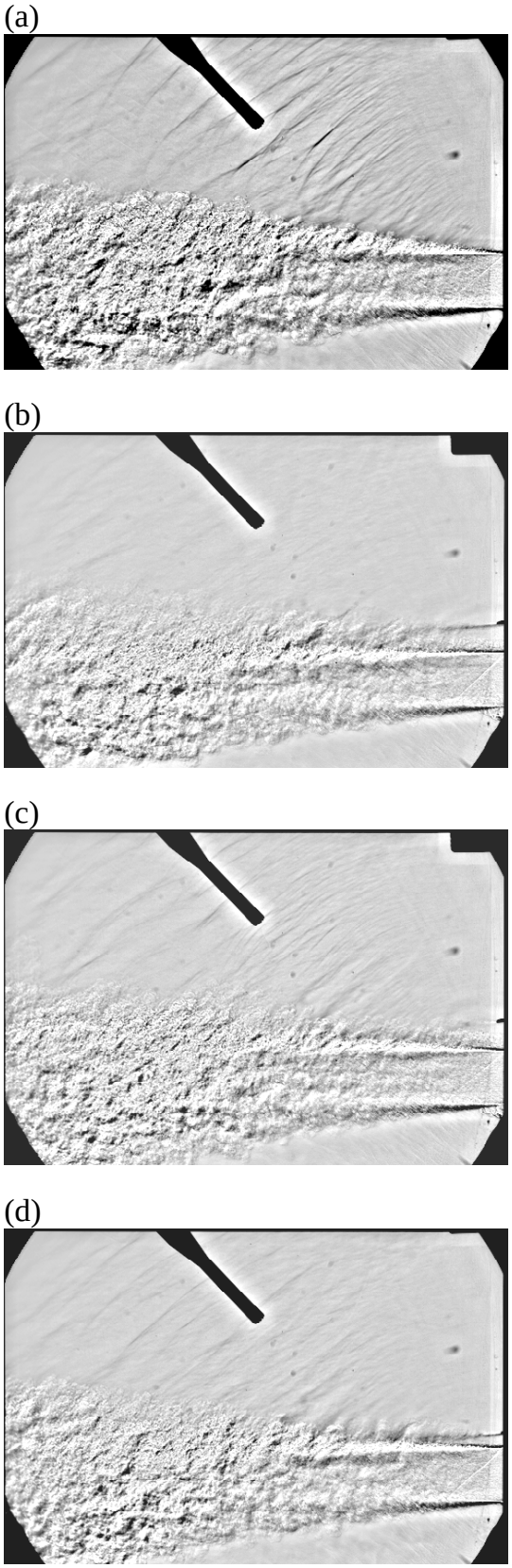

Fig.7 Selected spark schlieren pictures: (a) case A; (b) case G with h=7 mm; (c) case C with h=7 mm; (d) case G with h=3 mm.

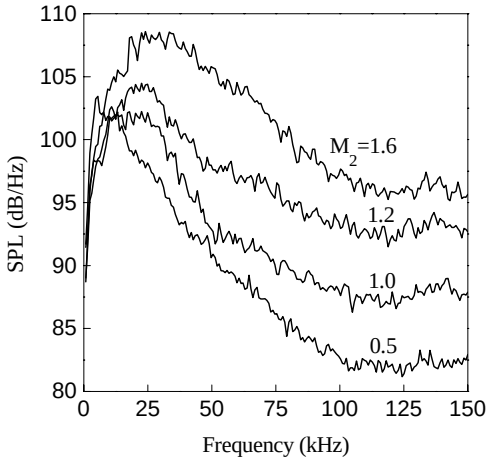

Fig.8 Microphone spectra for M_1=1.6, h=10 mm, and variable M_2.

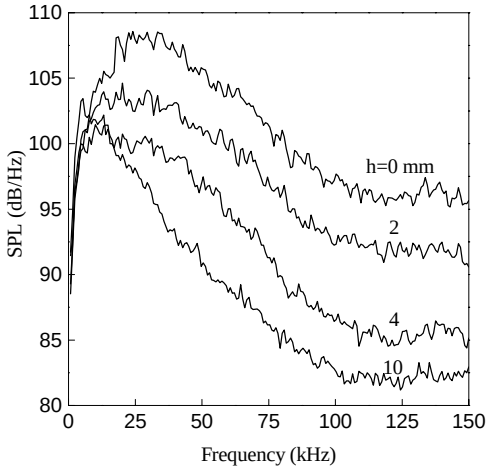

Fig.9 Microphone spectra for M_1=1.6, M_2=0.5, and variable h.

Noise spectra

Sound measurements were conducted inside an anechoic chamber, using a microphone with frequency response of 150 kHz. For a detailed description of the sound instrumentation and signal processing procedures, the reader is referred to Papamoschou & Debiasi [20]. The microphone tip was located 50 mm downstream of the jet exit and 35 mm above the jet centerplane. This position, shown in the pictures of Fig. 7, was chosen so that the microphone was inside the region of Mach wave emission from eddies near the jet exit, where the mean flow is relatively well-defined. The strongest Mach waves occur near the end of the potential core of the jet, where the flow is too complex to be characterized by the simple models constructed here. The microphone, as located in this experiment, did not pick up the strongest Mach waves. Therefore, the noise reduction discussed below cannot be extrapolated to the acoustic far field of the jet.

Figure 8 plots the noise spectra of cases A, C, D, and G with fixed secondary-flow height $h = 10$ mm. Decreasing M_2 results in reduction of all the spectral components except the very-low-frequency ones. The very-low-frequency noise may be related to quadrupole emission from the far field of the jet. At the frequency of 100 kHz, the flow with M_2=1.2 provides a 4-dB reduction while the flow with $M_2 = 0.6$ gives a 15-dB reduction. Figure 9 presents the effect of secondary-flow height h on the spectra of Case E (note that $h = 0$ means Case A). Increasing h allows a greater distance for the subsonic decay of the disturbance, hence leads to stronger noise reduction. It is evident that increasing the secondary-flow height beyond a certain value yields diminishing returns as the Mach wave reduction is so large that other noise sources become dominant. Another consideration, however, is that the secondary flow should be thick enough to cover the entire Mach-wave emitting region of the jet, not just the region near the exit. The optimum secondary-stream height should therefore be determined from far-field noise measurements.

Noise reduction

Since noise reduction depends on the nondimensional height βh, it is important to present the experimental results in terms of this parameter, rather than the actual height h. This is achievable by concentrating on a single frequency component, in this case the 100-kHz component. For $f = 100$ kHz and convective velocity $U_c = 550$ m/s (as predicted empirically), the wavenumber is $\beta = 2\pi f/U_c = 1.1$ mm^{-1}. The corresponding wavelength is 5.5 mm, which is in line with the spacing of the near-field Mach waves seen in Fig. 7(a). The microphone distance from the edge of the secondary flow is $\beta y \approx 10$ for the largest secondary flow and increases with decreasing secondary-flow height (recall that y is measured from the interface between the secondary and ambient flows). This places the microphone in the "far-field" for the purposes of comparing with the analytical estimates of sound reduction. The dependence of the noise reduction on βh and M_2 is shown in Fig. 10. For each secondary-flow height, noise declines gradually with decreasing M_2, the largest reductions occurring for subsonic M_2. Increasing the secondary-flow thickness produces a substantial benefit. The trends are similar to those seen in the ana-

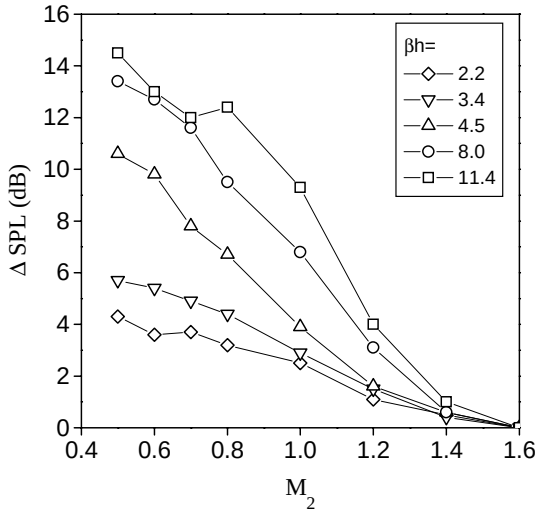

Fig.10 Experimental dependence of sound reduction on M_2 and βh.

lytical results of Fig. 5. Quantitatively, there is reasonable agreement between experiment and theory for $M_2 \geq 1$. For subsonic M_2, theory predicts much larger noise reduction than those recorded experimentally. This is not surprising because, as Mach waves are reduced by more than say 10 dB (69% reduction in rms pressure fluctuation), the other sources of noise–which are neglected by the theory– become increasingly more dominant. Another feature of the real case, not captured by the theory, is that a thin secondary flow dissipates much faster than does a thick one, therefore it covers only a small fraction of the Mach wave emitting region. Finally, we note that the structure of the Mach-wave emitting shear layer is likely to be three-dimensional [26], while the analysis treats it as two-dimensional. Despite these differences, the similarity between the analytical and experimental trends suggests that the primary noise reduction mechanism is the one described in this paper, i.e., a reduction of the disturbance magnitude at the point of origin combined with an exponential decay of the disturbance within the thickness of the secondary layer.

Conclusions

The intention of this paper was to explain at a fundamental level the noise reduction attained when a secondary flow is added around an otherwise Mach-wave-emitting supersonic jet. The interface between the primary and secondary streams was modeled as a flexible wavy wall with zero phase speed and arbitrary growth rate. The interface between the secondary and ambient streams was simulated by a vortex sheet. This arrangement allows one to study the effect of the secondary flow on Mach wave emission with all other parameters of the problem being fixed. The secondary stream, adjacent to the wavy wall, had variable Mach number and height. The semi-infinite ambient stream was supersonic. The vortex sheet motion consisted of the superposition of two components: the Kelvin-Helmholtz instability, and the reaction of the sheet to the presence of the wavy wall. For the conditions covered in this study, the first component did not radiate Mach waves while the second one did. A key result of the analysis is an expression for the amplitude of the second component of the vortex sheet motion, which describes the attenuating effect of the secondary stream on a disturbance generated by the wall. The study focused on the case of a subsonic secondary stream and compared it to the case of uniform supersonic flow over the wall. It was found that a subsonic layer over the wall creates two effects: first, the magnitude of the pressure disturbance on the wall is diminished; second, the disturbance decays exponentially within the height of the layer. The pressure fluctuation that is finally transmitted into the supersonic stream is very weak, leading to considerable noise suppression. The noise reduction increases with decreasing value of the secondary Mach number and with increasing height of the secondary flow. The level of noise reduction is only weakly dependent on wall growth rate. The theoretical trends compare favorably with experimental noise measurements in dual-stream jets consisting of a supersonic primary flow and a secondary flow with variable Mach number and height.

Acknowledgments

The support by NASA Langley Research Center is gratefully acknowledged (Grant NAG-1-2104 monitored by Mr. Thomas D. Norum). Ms. Erina Murakami is thanked for her assistance with the design and fabrication of the rectangular nozzle apparatus.

References

[1] J.M. Seiner and E. Krejsa, "Supersonic jet noise and the High Speed Civil Transport," AIAA 89-2358 (1989).

[2] C.K.W. Tam and P. Chen, "Turbulent mixing noise from supersonic jets," *AIAA J.* **32**, 1774 (1994).

[3] D.K. McLaughlin, G.D. Morrison, and T.R. Troutt, "Experiments on the instability waves in a supersonic jet and their acoustic radiation," *J. Fluid Mech.* **69**, 73, (1975).

[4] T.R. Troutt and D.K. McLaughlin, "Experiments on the flow and acoustic properties of a moderate Reynolds number supersonic jet, " *J. Fluid Mech.* **116**, 123, (1982).

[5] C.K.W. Tam and D.E. Burton, "Sound generated by instability waves of supersonic flows. Part 2. Axisymmetric Jets," *J. of Fluid Mech.* **138**, 249, (1984).

[6] J.M. Seiner, T.R.S Bhat, and M.K Ponton, "Mach wave emission from a high-temperature supersonic jet," *AIAA J.* **32**, 2345 (1994).

[7] B.E. Mitchell, S.K. Lele and P. Moin, "Direct computation of Mach wave radiation in an axisymmetric supersonic jet," *AIAA J.* **35**, 1574 (1997).

[8] C.C. Fenno, A. Bayliss, and L. Maestrello, "Interaction of sound from supersonic jets with nearby structures," *AIAA J.* **36**, 2153 (1998).

[9] R.R. Mankbadi, R. Hixon, S.-H. Shih, and L.A. Povinelli, "Use of linearized Euler equations for supersonic jet noise prediction, " *AIAA J.* **36**, 140 (1998).

[10] R. Westley and G.M. Lilley, "An investigation of the noise field from a small jet and methods for its reduction," College of Aeronautics, Report 53, Cranfield Univ., England, UK (1952).

[11] J.M. Seiner and M.M. Gilinski, "Nozzle thrust optimization while reducing jet noise," *AIAA J.* **35**, 420 (1997).

[12] K.K. Ahuja and W.H. Brown, "Shear flow control by mechanical tabs," AIAA-89-0994 (1989).

[13] M. Samimy, K.B.M.Q. Zaman, and M.F. Reeder, "Effect of tabs on the flow and noise control of an axisymmetric jet," *AIAA J.* **31**, 609 (1993).

[14] J.M. Seiner, and C.E. Grosch, "Mixing enhancement by tabs in round supersonic jets," AIAA-98-2326 (1998).

[15] Samimy, M., J.-H. Kim, , P.S. Clancy, and S. Martens, "Passive control of supersonic rectangular jets via nozzle trailing-edge modifications," *AIAA J.* **36**, 1230 (1998).

[16] P.J. Strykowski, A. Krothapalli, and S. Jendoubi, "The effect of counterflow on the development of compressible shear layers," *J. Fluid Mech.* **308**, 63 (1996).

[17] Tillman, T.G., Paterson, R.W., and Presz, W.M., "Supersonic nozzle mixer ejector," *J. Prop. Power* **8**, 513 (1992).

[18] K.B.M.Q. Zaman "Jet spreading by passive control and associated performance penalty," AIAA-99-3505 (1999)

[19] D. Papamoschou, "Mach wave elimination from supersonic jets, " *AIAA J.* **35**, 1604 (1997).

[20] D. Papamoschou and M. Debiasi, "Noise measurements in supersonic jets treated with the Mach wave elimination method," *AIAA J.* **37**, 154 (1999).

[21] Papamoschou, D. and Bunyajitradulya, A. "Evolution of large eddies in compressible shear layers," *Phys. Fluids* **4**, 756 (1997).

[22] E. Murakami, and D. Papamoschou, "PLIF investigation of coannular supersonic Jets," AIAA-98-3015 (1998)

[23] M.D. Dahl and P.J. Morris, "Noise from supersonic coaxial jets, Part 2: normal velocity profile," *J. Sound Vib.* **200**, 665 (1997).

[24] M.D. Dahl and P.J. Morris, "Noise from supersonic coaxial jets, Part 3: inverted velocity profile," *J. Sound Vib.* **200**, 701 (1997).

[25] L. Landau, "Stability of tangential discontinuities in compressible fluid, *Dokl. Akad. Nauk. SSSR,* **44**, 139 (1944).

[26] N.T. Clemens and M.G. Mungal, "Two- and three-dimensional effects in the supersonic mixing layer," *AIAA J.* **30**, 973 (1992).